Highlights

- Consideration of the different tensile and compressive moduli in I-beams
- Numerical assessment of flexural tests
- Local effects taken into account in the finite element method
- Assessment of the shear factor obtained analytically
- Good agreement between analytical and numerical results

NUMERICAL ASSESSMENT OF THE ANALYTICAL MODELS USED TO DETERMINE FLEXURAL AND SHEAR MODULI IN I-BEAMS WHEN THE TENSILE AND COMPRESSIVE MODULI ARE DIFFERENT

N. Insausti[a,*], I. Adarraga[a], N. Carbajal[a], F. Mujika[a]

[a]Materials + Technologies Group / Mechanics of Materials, Department of Mechanical Engineering, Faculty of Engineering of Gipuzkoa, University of the Basque Country (UPV/EHU) Plaza Europa, 1, 20018 Donostia-San Sebastián, Spain.

E-mail: nagore.insausti@ehu.eus

Abstract

The different compressive and tensile moduli of fibre reinforced composites have been considered in the analysis of the flexural and shear moduli of I-beams. Firstly, the neutral axis has been determined analytically and then, assuming that location of the neutral axis, the analytical flexural modulus of I-beams has also been obtained. In order to assess the proposed procedure, virtual pure bending and three-point bending tests at different spans have been carried out using the finite element method. The compressive and tensile moduli have been taken into account by defining two parts in the numerical models. The numerical flexural and shear moduli have been determined by reducing the data obtained in the virtual tests. Analytical and numerical results are in good agreement. Therefore, the flexural modulus determined by the proposed analytical approach can be introduced as a material property in the finite element method.

Key words: Tensile modulus; Compressive modulus; Flexural modulus; Shear modulus; Bending tests

---

1. Introduction

In unidirectional fibre reinforced composites the compressive and tensile moduli in the longitudinal direction are different. In particular, the tensile modulus is greater than the compressive modulus. The flexural modulus of the full-section is an intermediate value between the tensile and compressive moduli [1-4].

The dissimilar compressive and tensile performance of Carbon Fibre Reinforced Plastic (CFRP) composites has been analyzed in the last years [5-7]. According to Meng et al. [5] the increase of the repercussion of the unequal compressive and tensile moduli of CFRP composites is coupled with the growth of the thickness of the laminate. Furthermore, when the aforementioned moduli are not equal, the most accurate failure predictions are provided by strain failure criteria. Serna-Moreno et al. [6,7] focused on the three-point bending test of CFRP unidirectional and cross-ply laminates, respectively. These researches applied the homogenized section technique in order to obtain the analytical expressions which consider the different compressive and tensile moduli of the material.

Lee et al. [8] studied the difference of flexural and tensile moduli of FR4 substrates, which consist of woven-glass fabric and epoxy resin binder. This research determined the flexural modulus of flexible FR4 substrates using three-point bending tests, considering several span-to-depth ratios and the effect of temperature. The tensile modulus of the FR4 substrates was measured by means of direct tensile tests, through Digital Image Correlation (DIC) technique. The tensile modulus was greater than the flexural modulus.

When analyzing the bending performance of Fibre Reinforced Plastics (FRP), the inequality of compressive and tensile moduli has not frequently been taken into account. The flexural and shear behaviour of FRP pultruded profiles without considering the influence of the different compressive and tensile moduli has been widely analyzed [9-17].

Bank studied [9] the flexural and shear moduli of Glass Fibre Reinforced Plastic (GFRP) pultruded Wide Flange (WF) and I-beams concerning their full section by defining equivalent flexural and shear moduli. The shear coefficient was incorporated in the full section shear modulus. Then both equivalent moduli were obtained experimentally from three-point bending tests applying a linear regression. In this study the usage of Timoshenko beam theory was suggested in the design of thin-walled GFRP beams, in order to better estimate beam deflections and cost savings. Furthermore, experimental, analytical and numerical evaluations of the flexural stiffness of GFRP pultruded WF profiles were carried out by Neto and La Rovere [10]. Under those circumstances, the authors concluded that in the design of this type of beams Timoshenko beam theory, with mechanical properties estimated by Classical Lamination Theory (CLT), can be applied for the evaluation of the beam stiffness and for the verification of the deflections due to service loads. The shear modulus of pultruded FRP material and profiles obtained in several research papers was reviewed by Mottram [11]. In addition, a theoretical micromechanical modelling was developed in order to present an explanation of the great dispersion observed in the shear modulus values. Zhou and Hood [12] reported the bending behaviour concerning CFRP laminated I-beams. This research inferred that the web in-plane shear limited the correct experimental estimation of the sectional shear modulus. Additionally, Hayes and Lesko

[13,14] performed experimental and numerical tests in order to analyze the effect of warping and of transverse compressibility in the measurement of the Timoshenko shear stiffness of a simple solid beam and a pultruded double web beam. The influence of shear warping was found to be negligible whereas the boundary and loading conditions were shown to significantly affect the shear stiffness, since a decrease of the effective shear stiffness was observed at short spans.

The aforementioned investigations [9,11-14] were focused on symmetric three- and four-point bending tests of single-span pultruded GFRP beams. Recently, the flexural response of pultruded GFRP continuous beams has been analyzed by Turvey [15]. In this study closed-form shear deformation equations for forces and displacements of two-span continuous beams have been determined to predict the mid-span deflections, support rotations and surface strains. Furthermore, the predicted values have been compared with experimental ones.

Singh and Chawla [16] have recently evaluated pultruded FRP WF and I-beams material properties. The estimation of the elastic properties of such beams was performed experimentally and analytically. The shear coefficient was considered in the analysis and was determined by an approximate equation. Then, those properties were adopted in the Finite Element (FE) numerical models for comparison purposes.

Furthermore, DIC technique was implemented for the characterization of shear deformation of FRP composite beams by Berube et al. [17]. The objective of this study was to simultaneously measure the flexural and shear moduli of FRP beams during bending tests. In particular, marine-grade FRP composites reinforced with woven

roving E-glass fabric with several span-to-thickness and width-to-thickness ratios were tested.

The aim of this study is to assess the analytic models used to reduce experimental data of mechanical tests in the case of I-beams, concerning two aspects. On the one hand, the approach that considers different tensile and compressive moduli and their relationship with the flexural modulus. On the other hand, the analytic approach used for reducing flexural data at different spans, in order to obtain flexural and out-of-plane shear moduli. Thus, virtual bending tests have been carried out using the finite element method. The elastic properties introduced in the models are determined by virtual bending tests and reducing data by analytic equations. Those equations include the local deformation effects related to point load application in the model [18], bending, shear and the difference between tensile and compressive moduli. Mujika et al. [19] proposed a method to obtain tensile, compressive and flexural moduli by flexural tests. A strain gage was placed on the surface of the specimen and it was tested in four-point bending far of failure loads. Carrying out two tests with the strain gage on the compressive and then on the tensile side, the relation between the tensile and compressive modulus was obtained. Based on the present study, a similar experimental procedure can be used in I beams for checking the influence of the difference between tensile and compressive moduli.

2. Analytical approach

2.1. Relationship between tensile, compressive and flexural moduli

The relationship between flexural, tensile and compressive moduli of a beam of rectangular cross-section was analyzed by Mujika et al. in [19].

Considering the I-beam cross-section shown in Fig. 1, the longitudinal normal strain ε_x at a distance z from the middle plane can be determined as:

$$\varepsilon_x = \kappa\left(z - z_{NA}\right) \tag{1}$$

Where κ is the curvature, z is the coordinate measured from the middle plane and z_{NA} is the coordinate of the neutral axis, both being positive downwards, as shown in Fig. 1.

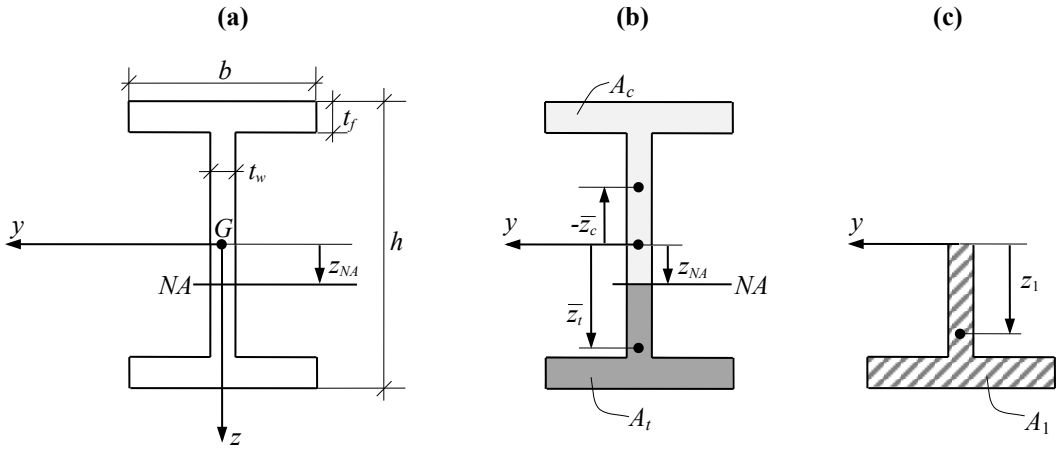

Fig. 1. (a) I-beam cross-section and coordinate reference system; (b) subareas in compression and tension; (c) half of the I-beam cross-section

Consequently, the longitudinal normal stresses can be defined as:

$$\sigma_x = E_i \varepsilon_x \quad i = c, t \tag{2}$$

Where E_i is the longitudinal modulus relative to the compressive side when $i = c$ and relative to the tensile side when $i = t$.

Since in pure bending the axial resultant force is zero, replacing stress-strain relationships from Eq. (2), it results:

$$0 = \int_A \sigma_x dA = \kappa E_c \int_{A_c} \left(z - z_{NA}\right) dA_c + \kappa E_t \int_{A_t} \left(z - z_{NA}\right) dA_t \tag{3}$$

Where A_c and A_t are the subareas in compression and in tension, respectively.

Defining the ratio between the tensile and compressive moduli as $\lambda = E_t / E_c$, Eq. (3) can be written as:

$$\int_{A_c} (z - z_{NA}) dA_c + \lambda \int_{A_t} (z - z_{NA}) dA_t = 0 \tag{4}$$

The integrands in Eq. (4) are the first moments of area of the compression and tension surfaces with respect to the neutral axis.

Eq. (4) can be written as:

$$A_c \overline{z_c} + A_t \overline{z_t} = 0 \tag{5}$$

Where $\overline{z_c}$ and $\overline{z_t}$ are the coordinates of the centres of gravity of the subareas in compression and in tension, respectively, in the reference system shown in Fig. 1.

Additionally, the first moments of area can be defined as:

$$\begin{aligned} A_c \overline{z_c} &= -A_1 z_1 + \frac{b}{2} z_{NA}^2 \\ A_t \overline{z_t} &= A_1 z_1 - \frac{b}{2} z_{NA}^2 \end{aligned} \tag{6}$$

Being A_1 half the surface of the cross-section and z_1 the coordinate of the gravity centre of the half of the I-beam cross-section, as shown in Fig. 1c.

The subareas under compression and tension can be expressed as:

$$\begin{aligned} A_c &= A_1 + b z_{NA} \\ A_t &= A_1 - b z_{NA} \end{aligned} \tag{7}$$

Taking into consideration Eqs. (5) to (7), Eq. (4) results:

$$\frac{1}{2} b (\lambda - 1) z_{NA}^2 - z_{NA} A_1 (\lambda + 1) + (\lambda - 1) A_1 z_1 = 0 \tag{8}$$

Solving for z_{NA} in Eq. (8):

$$z_{NA} = \frac{1}{2}\left[\frac{2A_1}{b}\frac{\lambda+1}{\lambda-1} \pm \sqrt{\frac{4A_1^2}{b^2}\frac{(\lambda+1)^2}{(\lambda-1)^2} - \frac{8A_1}{b}z_1} \right] \tag{9}$$

The first summand tends to ∞ when $\lambda \to 1$. Therefore, only the negative sign has sense.

Then, the coordinate of the neutral axis can be determined from:

$$z_{NA} = \frac{A_1}{b}\frac{\lambda+1}{\lambda-1} - \sqrt{\frac{A_1}{b}\left(\frac{A_1}{b}\left(\frac{\lambda+1}{\lambda-1} \right)^2 - 2z_1 \right)} \tag{10}$$

According to Eq. (10) $\lim_{\lambda \to 1} z_{NA} = 0$, as expected.

Eq. (10) can be applied to the particular case of a rectangular section:

$$\begin{aligned} A_1 &= \frac{1}{2}bh \\ z_1 &= \frac{h}{4} \end{aligned} \tag{11}$$

Replacing Eq. (11) in Eq. (10), it results:

$$z_{NA} = \frac{h}{2}\frac{\sqrt{\lambda}-1}{\sqrt{\lambda}+1} \tag{12}$$

The result of Eq. (12) is the same as that obtained in [5].

On the other hand, taking into account that the resultant moment of the normal stresses is the bending moment *M*:

$$M = \int_A \sigma_x z dA = \int_{A_c} \sigma_x z dA_c + \int_{A_t} \sigma_x z dA_t \tag{13}$$

Replacing stress-strain relationships from Eq. (2) into Eq. (13):

$$M = \kappa E_c \int_{A_c} (z - z_{NA}) z dA_c + \kappa E_t \int_{A_t} (z - z_{NA}) z dA_t \tag{14}$$

Rearranging terms, Eq. (14) results:

$$\frac{M}{\kappa E_c} = \int_{A_c} z^2 dA_c - z_{NA} \int_{A_c} z dA_c + \lambda \left[\int_{A_t} z^2 dA_t - z_{NA} \int_{A_t} z dA_t \right] \tag{15}$$

Since the integrands in Eq. (15) are the second and first moments of area of the compression and tension surfaces with respect to the neutral axis, Eq. (15) can be written as:

$$\frac{M}{\kappa E_c} = I_y^c - z_{NA} A_c \overline{z_c} + \lambda \left[I_y^t - z_{NA} A_t \overline{z_t} \right] \tag{16}$$

Where

$$\begin{aligned} I_y^c &= I_{y1} + \frac{1}{3} b z_{NA}^3 \\ I_y^t &= I_{y1} - \frac{1}{3} b z_{NA}^3 \end{aligned} \tag{17}$$

I_y^c and I_y^t are the second moment of area of the compression surface and the tensile surface, respectively. Being

$$I_{y1} = \frac{1}{2} I_y \tag{18}$$

where I_y is the second moment of area of the whole section.

According to Classical Beam Theory (CBT), the curvature is given by:

$$\frac{M}{E_f I_y} = \kappa \tag{19}$$

Where E_f is the flexural modulus.

Comparing Eqs. (16) and (19):

$$\frac{M}{E_c B} = \frac{M}{E_f I_y} \tag{20}$$

Where $B = I_y^c - z_{NA} A_c \overline{z_c} + \lambda \left[I_y^t - z_{NA} A_t \overline{z_t} \right]$.

Therefore, when the tensile and compressive moduli are different, the flexural modulus E_f can be obtained analytically from Eq. (20) as:

$$E_f = \frac{E_c B}{I_y} \tag{21}$$

The expression given in Eq. (21) is valid also for the case of a rectangular section, as expected:

$$E_f = \frac{4\lambda}{\left(1+\sqrt{\lambda}\right)^2} E_c \tag{22}$$

According to Eq. (22) the flexural modulus does not depend on the dimensions of the rectangular section. After a parametric study, it can be seen that in the case of an I-beam the dependence on the dimensions of Fig. 1 is small. Moreover, the values are close to those obtained for a rectangular section.

2.2. Determination of the flexural modulus in pure bending

The procedure followed to determine the flexural modulus in pure bending is described in this section.

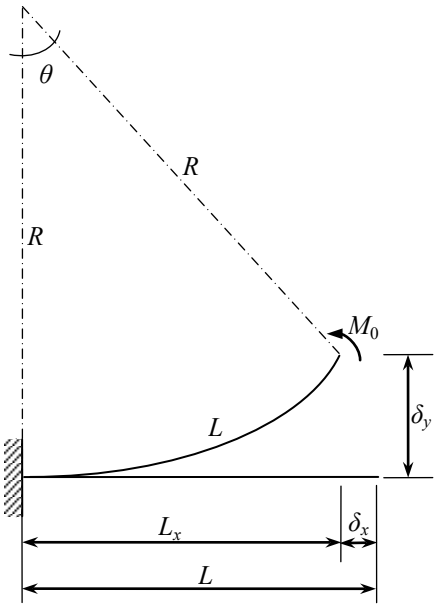

Fig. 2. Original and deformed shape of the beam subjected to pure bending

In pure bending, the elastic curve is a circumference, as shown in Fig. 2. Therefore, the horizontal and vertical displacements of the beam, δ_x and δ_y, respectively, can be defined as:

$$\begin{aligned} \delta_x &= L - R\sin\theta \\ \delta_y &= R\left(1-\cos\theta\right) \end{aligned} \tag{23}$$

Where L is the length of the beam, R is the radius of curvature and θ is the rotation angle. If δ_x and δ_y are known, the radius of curvature and the rotation angle, can be calculated by solving Eq. (23). Taking into account that the curvature is the inverse of the radius of curvature, the next expression is fulfilled:

$$E_f = \frac{M_0 R}{I_y} \tag{24}$$

2.3. Determination of the flexural and shear moduli in three-point bending

Mujika [18] proposed a procedure for determining the flexural and out-of-plane shear moduli carrying out three-point bending tests at different spans. The experimental displacement given by the testing machine was used and consequently local deformation effects were incorporated. Those effects include the deformation of the specimen in the thickness and the inherent deformability of components of the test setup. It has been seen that the main dependence is related to the load cell stiffness [20]. The resultant equation of the displacement was a third order polynomial. When the displacement is directly measured in the specimen by an external device, the local deformation effects have not influence and a linear regression can be used [9].

In the present study, virtual tests have substituted experiments. The goal of these virtual tests is to replicate the procedure followed in experimental practice. Thus, in the FE models, loads are concentrated and consequently a local deformation occurs in the thickness direction of the mesh near the load application, in a similar manner as in actual experiments, as it can be seen in Fig. 3. In the case of the numerical model, the local deformation depends on the mesh size. Therefore, local deformation effects are present in both cases, actual experiments and FE analyses, although there is no relationship between both effects. Indeed, in the experimental case those effects include also the inherent deformability of the test setup. In both cases, numerical and experimental, all deformation effects that are not related to the bending and shear of the specimen are named local deformation effects and are included in a stiffness term represented by a spring in the analytic approach.

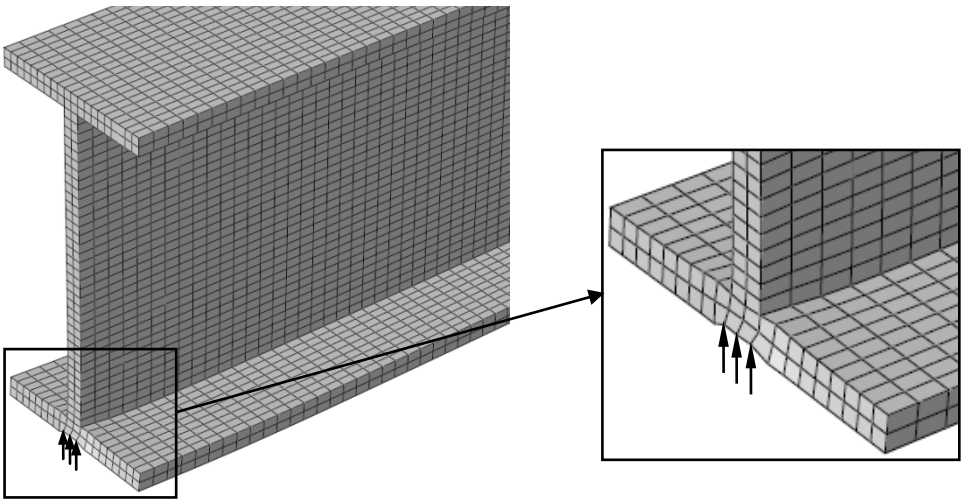

Fig. 3. Local deformation on the I-beam

Considering the symmetry conditions of the three-point bending test, half of the beam has been modelled, as shown in Fig. 4. In the analytic model, a spring has been incorporated in order to consider the local deformation effects of the FE mesh, presented in Fig. 3.

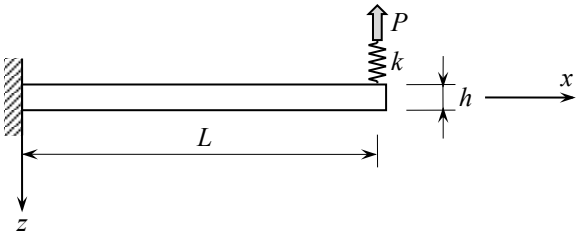

Fig. 4. Model of the three-point bending test including local deformation effects

If bending, shear and the spring are considered, the complementary strain energy U^* of the cantilever beam with a point load can be determined as:

$$U^* = \int_L \frac{M^2}{2E_f I_y} dl + \chi \int_L \frac{V^2}{2G_{13} A} dl + \frac{P^2}{2k} \tag{25}$$

Where M is the bending moment, V is the shear force, P is the force at the support, E_f is the flexural modulus, G_{13} is the out-of-plane shear modulus, I_y is the second moment of area, A is the cross-sectional area, χ is the shear correction factor and k is the stiffness of the numerical model that includes local deformation effects. These effects are similar to those present in experiments, even though the numerical stiffness has no relation with the experimental stiffness that depends on the specimen and the testing system characteristics.

The shear correction factor is a coefficient that depends on the geometry of the section and comes from the fact that the shear stress distribution is parabolic [4]. It is given by:

$$\chi = \frac{A}{I_y^2} \int_A \frac{Q_y^2}{w^2} dA \tag{26}$$

being Q_y the first moment of area and w the width, which is variable in the case of the I section and $w = b$ in the case of the rectangular section.

According to the theorem of Engesser-Castigliano [21], the displacement δ of the loading point section is:

$$\delta = \frac{\partial U^*}{\partial P} = \int_L \frac{MM'}{E_f I_y} dl + \chi \int_L \frac{VV'}{G_{13} A} dl + \frac{PP'}{k} = \frac{4PL^3}{E_f \lambda_I h^3} + \chi \frac{PL}{G_{13} \lambda_A h} + \frac{P}{k} \tag{27}$$

Being the parameters in Eq. (27):

$$\begin{aligned} &\lambda_A = 2b\lambda_f + t_w\left(1-2\lambda_f\right) \Rightarrow A = \lambda_A h \\ &\lambda_I = b - \left(b - t_w\right)\left(1-2\lambda_f\right)^3 \Rightarrow I_y = \frac{1}{12}\lambda_I h^3 \end{aligned} \tag{28}$$

Where A is the area of the cross-section, I_y is the second moment of area, $\lambda_f = t_f / h$, b is the width of the flanges, h is the height and t_f and t_w are the flange and web thicknesses, respectively, as shown in Fig. 1. When a rectangular cross-section is concerned $\lambda_f = 1 \Rightarrow \lambda_A = \lambda_I = b$ and $\chi = 6/5$.

Rearranging terms, it results:

$$\delta = \frac{4PL^3}{E_f \lambda_I h^3}\left[1 + \frac{\chi}{4}\frac{\lambda_I}{\lambda_A}\frac{E_f}{G_{13}}\left(\frac{h}{L}\right)^2 + \frac{E_f \lambda_I}{4k}\left(\frac{h}{L}\right)^3\right] \tag{29}$$

Eq. (29) can be written as:

$$E_f = \frac{4mL^3}{\lambda_I h^3}\left[1 + \frac{\chi}{4}\frac{\lambda_I}{\lambda_A}\frac{E_f}{G_{13}}\left(\frac{h}{L}\right)^2 + \frac{E_f \lambda_I}{4k}\left(\frac{h}{L}\right)^3\right] \tag{30}$$

Where $m = P/\delta$ is the slope of the load-displacement curve.

Eq. (30) can be expressed as:

$$E_0^{-1} = E_f^{-1}\left[1 + \frac{\chi}{4}\frac{\lambda_I}{\lambda_A}\frac{E_f}{G_{13}}\left(\frac{h}{L}\right)^2 + \frac{E_f \lambda_I}{4k}\left(\frac{h}{L}\right)^3\right] \tag{31}$$

where

$$E_0 = \frac{4mL^3}{\lambda_I h^3} \tag{32}$$

Eq. (31) is equivalent to a polynomial of third order:

$$y = A_R + B_R x^2 + C_R x^3 \tag{33}$$

Where:

$$y = E_0^{-1}, \quad \text{x}=\frac{h}{L}, \quad A_R = E_f^{-1}, \quad B_R = \frac{\chi}{4}\frac{\lambda_I}{\lambda_A} G_{13}^{-1}, \quad C_R = \frac{\lambda_I}{4} k^{-1} \tag{34}$$

The subindex *R* in Eqs. (33) and (34) is related to regression.

When *n* numerical values of the slope *m* concerning different spans are achieved, the minimum squares method is employed in order to determine the coefficients A_R, B_R and C_R of Eq. (33) [18]. Once those coefficients have been obtained, E_f, G_{13} and *k* are:

$$E_f = A_R^{-1}, \quad G_{13} = \frac{\chi}{4}\frac{\lambda_I}{\lambda_A} B_R^{-1}, \quad k = \frac{\lambda_I}{4} C_R^{-1} \tag{35}$$

It is worth noting that the value of *k* is not introduced directly in the numerical analysis models. It is a result due to the use of concentrated loads in the finite element method as shown in Fig. 3.

3. Numerical analysis

3.1. Input data

A rectangular cross-section beam and an I-beam have been modelled. The geometrical features considered are those shown in Fig. 5. The I-beam cross-section has a total height of 120 mm, the width of the flanges is of 60 mm and the thickness for both, web and flanges, is of 6 mm. In the case of the rectangular cross-section beam the width is of 10 mm and the thickness of 6 mm, in representation of a coupon of the I-beam.

The mechanical properties considered in the FE numerical analyses, which are shown in Table 1, correspond to a GFRP pultruded beam [22].

Table 1. Mechanical properties of GFRP pultruded beam

E_t (GPa)	E_c (GPa)	E_2, E_3 (GPa)	G_{12}, G_{13} (GPa)	G_{23} (GPa)	ν_{12}, ν_{13}	ν_{23}
39.9	25.3	8.3	3.6	3.7	0.27	0.11

The neutral axis location has been determined analytically according to Eq. (10). This value has been taken into consideration when defining the corresponding cross-section in the FE model. With this aim, the beams have been modelled adopting two different parts. In the upper part or the subarea in compression, the compressive modulus E_c, and in the lower part or the subarea in tension, the tensile modulus E_t, have been introduced. The two subareas are represented in Fig. 5. In the FE models, the symmetry conditions have been taken into account and, consequently, all the displacements have been restricted in $x = 0$ section.

Eight-node linear solid elements with incompatible modes (C3D8I) have been employed in ABAQUS Standard [23]. These elements have been selected due to the improvement of the results when shear influence is important [24]. The approximate size of the elements has been of 1 x 0.25 x 1 mm in the rectangular section and of 3 x 3 x 5 mm in the I-beam. As far as pure bending virtual tests are concerned, the number of C3D8I elements of the rectangular section beam model has been of 96000 and in the case of the I-beam of 63720. In the three-point bending models, the minimum number of C3D8I elements when the rectangular cross-section is concerned has been of 4800 and the maximum of 14400, due to the shorter length of the beams. In the case of the I-beam model, the minimum number of C3D8I elements has been 18240 and the

maximum 66576. In the case of pure bending the convergence was reached with greater element sizes, nevertheless, it has been necessary to use the aforementioned element sizes in order to obtain adequate values of the shear modulus.

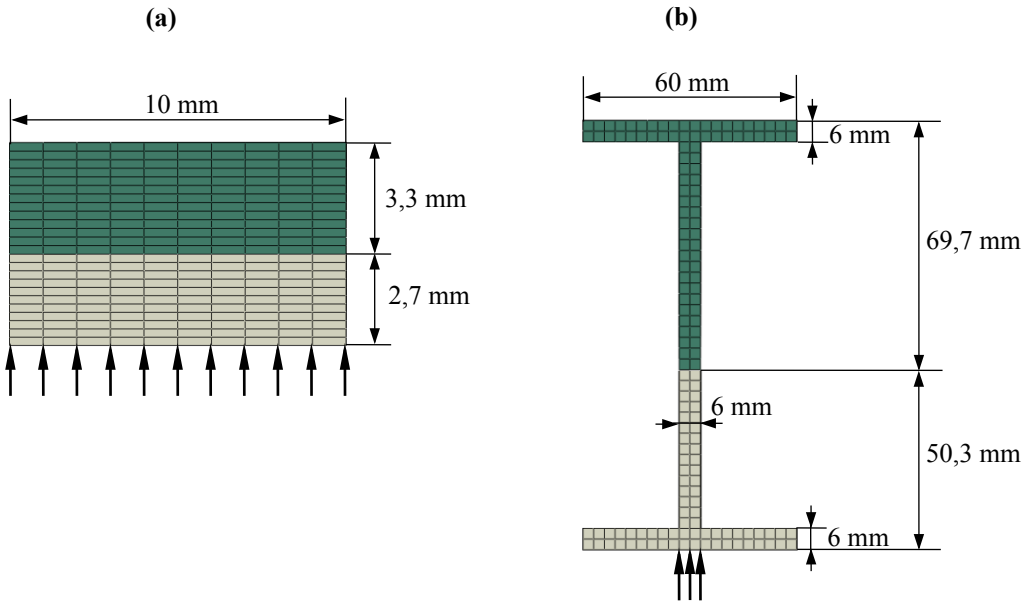

Fig. 5. Dimensions, loading and mesh with different compressive and tensile moduli; a) rectangular cross-section; b) I cross-section

3.2. Results of pure bending

A rectangular cross-section beam and I-beam have been modelled in pure bending in order to compare the numerically obtained flexural modulus to that calculated analytically.

On the one hand, the flexural modulus has been obtained analytically, from Eq. (21). On the other hand, a pure bending test has been numerically simulated, as seen in Fig. 6. The numerical displacements have been achieved in section 1 shown in Fig. 6, since in this section the effect of the point load application is considered negligible. The number of C3D8I elements and the longitudinal dimensions used in the models are shown in Table 2. In the case of the I-beam the longitudinal dimension of the elements has been

increased progressively from section 1 towards the campled section from 5 mm to 20 mm.

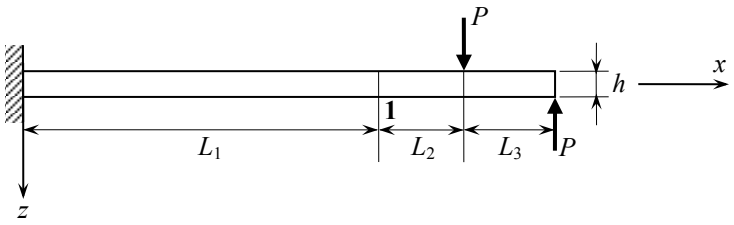

Fig. 6. Scheme of the pure bending model

Table 2. Length of the beams and number of elements considered in the FE models

	L_1 (mm)	L_2 (mm)	L_3 (mm)	Number of elements
Rectangular cross-section	250	100	50	96000
I cross-section	2500	1000	500	63720

The radius of curvature R and the rotation angle θ have been determined with the horizontal and vertical displacements δ_x and δ_y of section 1 obtained numerically from FE analyses (Fig. 2). Then, the flexural modulus has been achieved from Eq. (24).

The values of the flexural modulus concerning the rectangular cross-section and the I-beam are shown in Table 3, where the analytically predicted and numerically calculated values are very similar. Indeed, the relative error between the analytical and the numerical values is lower than 1 %. In addition, the flexural modulus determined according to the analytical procedure described in this work and defined in Eq. (21) has been introduced directly as an input value, for both parts, in FE models and it has been verified that the output flexural modulus has been the same as the input value.

Table 3. Analytical and numerical values of the flexural modulus

	E_f (MPa)		
	Analytical	Numerical	Difference (%)
Rectangular cross-section	31364	31449	0.27
I cross-section	31213	31264	-0.16

3.3. Results of three-point bending

Three-dimensional models of rectangular and I-beam cross-sections have been implemented in ABAQUS standard. After symmetry considerations, half of the beam has been modelled and, hence, a cantilever beam has been analyzed. In order to take into account the unequal compressive and tensile moduli, the implemented models include the aforementioned two parts, the upper part with compressive elastic modulus and the lower part with tensile elastic modulus.

As far as the geometrical features are concerned, they are the same as those stated in section 3.1, which are shown in Fig. 5. In this case, five different beam lengths have been considered. When modelling the rectangular cross-section the following lengths have been implemented L = 20, 24, 30, 40 and 60 mm with the dimensions shown in Fig. 5. Those are the semi-spans of the simulated tests, since due to symmetry half of the beam has been modelled. These spans were selected with the condition that the differences between the independent variables of the regression (h / L) were kept constant. With regard to the I-beam the five semi-spans analyzed in the FE models are L = 600, 750, 1000, 1500 and 3000 mm. As the length of the beams is variable, the number of C3D8I elements of the FE models is also different for each case. As far as the rectangular section is concerned, the minimum number of elements has been of 4800 and the maximum of 14400. In the case of the I-beam the minimum number of elements considered has been of 18240 and the maximum of 66576.

The shear correction factor concerning this I-beam section has been determined according to Eq. (26):

$$\chi = \chi_{\text{web}} + \chi_{\text{flanges}} = 1.96 + 0.08 = 2.04 \tag{36}$$

According to Eq. (36), the main contribution to the shear correction factor comes from the web. It is worth noting that usually the shear factor is incorporated into the shear modulus. The modulus so obtained is defined as the "section modulus" [9]. In the present study, as the shear modulus is introduced in the model as a material property, the suitability of the shear factor is also checked.

A fixed displacement of value L / 50 has been imposed at the free end of the beam in the FE models. For each of the different lengths, the slope of the load-displacement curve has been determined as the reaction force divided by the fixed displacement. E_0 has been obtained according to the expression shown in Eq (32) and a third order regression has been applied to the five values.

The values of E_0 obtained by FE and the regression curves are shown in Fig. 7 for both sections. According to Eq. (29), the whole displacement of the end point of the beam is due to bending, shear and local deformation. Fig. 8 shows the variation of the percentage of shear and local effects related to the total flexural displacement, for the five semi-spans considered in the analysis.

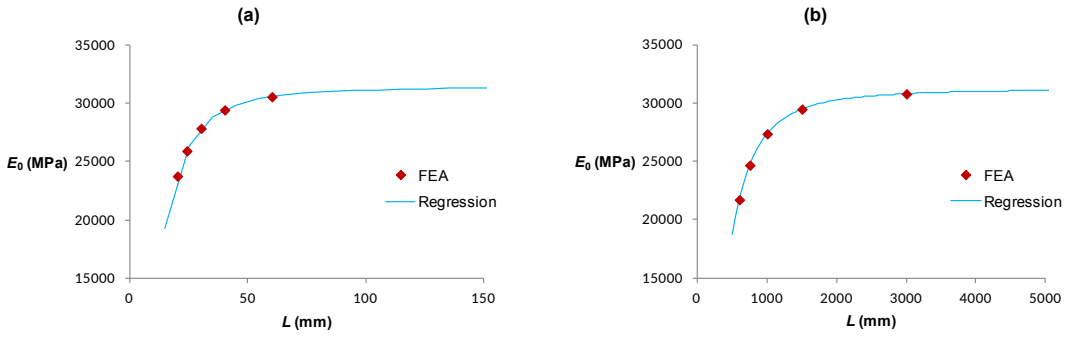

Fig. 7. Variation of E_0 with respect to the semi-span; a) rectangular cross-section, b) I cross-section

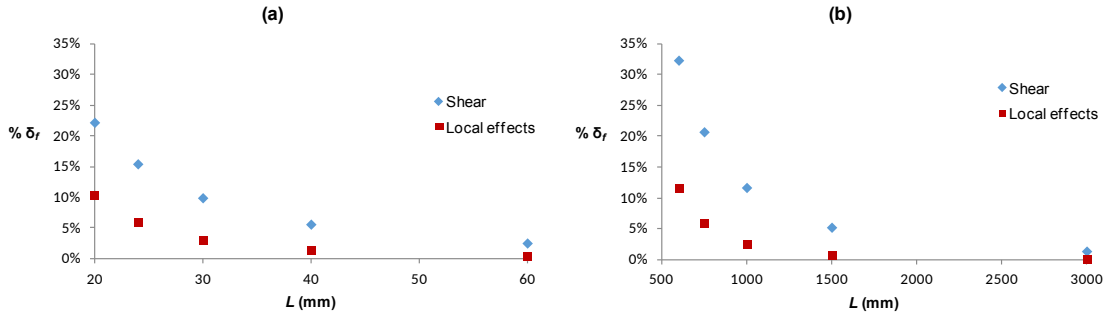

Fig. 8. Percentage of shear and local effects rate relative to the total of flexural displacement of the beam versus the semi-span; a) rectangular cross-section, b) I cross-section

Finally, the flexural and shear moduli and system stiffness values obtained by FE and third order regression concerning both rectangular cross-section and I-beam are shown in Table 4. FE input values of tensile and compressive longitudinal and out-of-plane shear moduli and the flexural modulus obtained according to Eq. (21) are also included. The agreement between the input and numerical values is better for the I-beam than for the rectangular cross-section beam, probably due to the greater influence of shear in that case, as seen in Fig. 8. The system stiffness is greater in the rectangular cross-section beams, due to the greater load application length, as seen in Fig. 5.

Table 4. Flexural and shear moduli obtained via FE and third order regression considering different compressive and tensile moduli

	Input FE			Analytical	Virtual experiments		
	E_t (MPa)	E_c (MPa)	G_{13} (MPa)	E_f (MPa)	E_f (MPa)	G_{13} (MPa)	k (N/mm)
Rectangular cross-section	39900	25300	3600	31364	31412	3836	20762
I cross-section	39900	25300	3600	31213	31222	3567	11208

Then the flexural modulus obtained analytically has been introduced in the numerical models in order to carry out virtual experiments with a unique part using the flexural modulus instead of two parts with the compressive and tensile moduli. The relative

difference between the analytical values of both moduli and those obtained from the virtual experiments is shown in Table 5. This difference is greater in the case of the out-of-plane shear modulus than in the case of flexural modulus and is maximum in the rectangular section case. The I-beam analytical and numerical results show very good agreement.

Table 5. Difference between the flexural and shear moduli input values and those obtained numerically via FE and third order regression considering only the flexural modulus

	Input E_f (MPa)	Numerical E_f (MPa)	Difference (%)	Input G_{13} (MPa)	Numerical G_{13} (MPa)	Difference (%)
Rectangular cross-section	31364	31411	0.15	3600	3828	6.33
I cross-section	31213	31223	0.03	3600	3566	-0.94

4. Summary and conclusions

The flexural modulus of FRP I cross-section beams has been analyzed taking into consideration the inequality of compressive and tensile moduli. The location of the neutral axis and the flexural modulus have been determined analytically as a function of the relation between tensile and compressive moduli.

Then finite element analyses have been carried out, not only concerning pure bending but also regarding three-point bending at different spans. Compression and tension parts have been defined depending on the neutral axis position determined from the analytic approach. The shear factor has been determined analytically and the numerical data have been reduced by applying the analytical approaches of pure bending and three-point bending.

Results have shown that the flexural modulus determined analytically and numerically are in good agreement in both pure and three-point bending. The shear modulus

resulting from the virtual three-point bending tests at different spans is also in good agreement with that introduced as input value. In that case, it is important to include the local deformation effects, related to the application of concentrated loads in the finite element model.

Therefore, in order to determine accurately the flexural and out-of-plane shear moduli, the importance of performing flexural tests at different spans and of considering the local effects has been shown. Additionally, when the tensile and compressive moduli are known, the flexural modulus determined applying the analytical procedure described in this paper can be directly introduced as a material property in the finite element analysis of bending dominated problems.

From an experimental point of view, if two tests are performed placing one strain gage on the compressive side and then on the tensile side, the relationship between the compressive and tensile modulus can be obtained. Using the equations of the approach proposed in the current study, it would be enough to use a single strain gage to determine the compressive, tensile and flexural moduli of I-beams in a simple manner.

Acknowledgements

The financial support of the University of the Basque Country (UPV/EHU) in the Research Group GIU 16/51 “Mechanics of Materials” is gratefully acknowledged.

References

[1] R.M. Jones, Apparent Flexural Modulus and Strength of Multimodulus Materials, J. Composite Mater. 10 (1976) 342-354.
[2] G. Zhou, G.A.O. Davies, Characterization of thick glass woven roving/polyester laminates: 2. Flexure and statistical considerations, Composites. 26 (1995) 587-596.
[3] S.G. Paolinelis, S.A. Paipetis, P.S. Theocaris, 3-Point Bending at Large Deflections of Beams with Different Moduli of Elasticity in Tension and Compression, Journal of Testing and Evaluation. 7 (1979) 177-182.
[4] J.M. Gere, S.P. Timoshenko, Mechanics of Materials, 4th ed., Pws, 1997.
[5] M. Meng, H.R. Le, M.J. Rizvi, S.M. Grove, The effects of unequal compressive/tensile moduli of composites, Composite Structures. 126 (2015) 207-215.
[6] M.C. Serna Moreno, A. Romero Gutiérrez, J.L. Martínez Vicente, Different response under tension and compression of unidirectional carbon fibre laminates in a three-point bending test, Composite Structures. 136 (2016) 706-711.
[7] M.C. Serna Moreno, A. Romero Gutiérrez, J.L. Martínez Vicente, First flexural and interlaminar shear failure in symmetric cross-ply carbon-fibre laminates with different response under tension and compression, Composite Structures. 146 (2016) 62-68.
[8] T. Lee, C. Kim, M.S. Kim, T. Kim, Flexural and tensile moduli of flexible FR4 substrates, Polymer Testing. 53 (2016) 70-76.
[9] L. Bank, Flexural and Shear Moduli of Full-Section Fiber Reinforced Plastic (FRP) Pultruded Beams, Journal of Testing and Evaluation. 17 (1989) 40-45.
[10] A.B.S.S. Neto, H.L. La Rovere, Flexural stiffness characterization of fiber reinforced plastic (FRP) pultruded beams, Composite Structures. 81 (2007) 274-282.
[11] J.T. Mottram, Shear Modulus of Standard Pultruded Fiber Reinforced Plastic Material, J. Composite Constr. 8 (2004) 141-147.
[12] G. Zhou, J. Hood, Design, manufacture and evaluation of laminated carbon/epoxy I-beams in bending, Composites Part A: Applied Science and Manufacturing. 37 (2006) 506-517.
[13] M.D. Hayes, J.J. Lesko, Measurement of the Timoshenko Shear Stiffness. I: Effect of Warping, J. Composite Constr. 11 (2007) 336-342.
[14] M.D. Hayes, J.J. Lesko, Measurement of the Timoshenko Shear Stiffness. II: Effect of Transverse Compressibility, J. Composite Constr. 11 (2007) 343-349.
[15] G.J. Turvey, Testing and analysis of pultruded GFRP continuous beams for the deflection serviceability limit state, Composite Structures. 141 (2016) 213-220.
[16] S.B. Singh, H. Chawla, An investigation of material characterization of pultruded FRP H- and I-beams, Mechanics of Advanced Materials and Structures. 25 (2018) 124-142.
[17] K.A. Berube, R.A. Lopez-Anido, A.J. Goupee, Determining the Flexural and Shear Moduli of Fiber-Reinforced Polymer Composites Using Three-Dimensional Digital Image Correlation, Exp Techniques. 40 (2016) 1263-1273.
[18] F. Mujika, On the effect of shear and local deformation in three-point bending tests, Polymer Testing. 26 (2007) 869-877.
[19] F. Mujika, N. Carbajal, A. Arrese, I. Mondragon, Determination of tensile and compressive moduli by flexural tests, Polymer Testing. 25 (2006) 766-771.
[20] F. Mujika, A. Arrese, I. Adarraga, U. Oses, New correction terms concerning three-point and four-point bending tests, Polymer Testing. 55 (2016) 25-37.
[21] J.T. Oden, E.A. Ripperger, Mechanics of Elastic Structures, 2nd edition ed., Hemisphere Publishing Corporation, Washington, 1981.

[22] T. Morgado, N. Silvestre, J.R. Correia, Simulation of fire resistance behaviour of pultruded GFRP beams – Part I: Models description and kinematic issues, Composite Structures. 187 (2018) 269-280.
[23] Dassault Systèmes Simulia Corp., Commercial software ABAQUS Standard, version 6.12, (2012).
[24] Dassault Systèmes Simulia Corp., ABAQUS Theory Manual, 6.12, (2012).